



Titre: Adaptive point learning with uncertainty quantification to generate margin lines on prepared teeth
Title:

Auteurs: Ammar Alsheghri, Yoan Ladini, Golriz Hosseinimanesh, Farida Cheriet, Imane Chafi, François Guibault, & Julia Kerem
Authors:

Date: 2024

Type: Article de revue / Article

Référence: Alsheghri, A., Ladini, Y., Hosseinimanesh, G., Cheriet, F., Chafi, I., Guibault, F., & Kerem, J. (2024). Adaptive point learning with uncertainty quantification to generate margin lines on prepared teeth. Applied Sciences, 14(20), 9486 (21 pages). <https://doi.org/10.3390/app14209486>
Citation:

Document en libre accès dans PolyPublie

Open Access document in PolyPublie

URL de PolyPublie: <https://publications.polymtl.ca/59628/>
PolyPublie URL:

Version: Version officielle de l'éditeur / Published version
Révisé par les pairs / Refereed

Conditions d'utilisation: CC BY
Terms of Use:

Document publié chez l'éditeur officiel

Document issued by the official publisher

Titre de la revue: Applied Sciences (vol. 14, no. 20)
Journal Title:



Maison d'édition: Multidisciplinary Digital Publishing Institute
Publisher:

URL officiel: <https://doi.org/10.3390/app14209486>
Official URL:

Mention légale: © 2024 by the authors. Licensee MDPI, Basel, Switzerland. This article is an open access article distributed under the terms and conditions of the Creative Commons Attribution (CC BY) license (<https://creativecommons.org/licenses/by/4.0/>).
Legal notice:

Article

Adaptive Point Learning with Uncertainty Quantification to Generate Margin Lines on Prepared Teeth

Ammar Alsheghri ^{1,2,*} , Yoan Ladini ³, Golriz Hosseinimanesh ³, Imane Chafi ³, Julia Keren ⁴, Farida Cheriet ³  and François Guibault ^{3,*}

¹ Mechanical Engineering Department, King Fahd University of Petroleum and Minerals (KFUPM), Dhahran 31261, Saudi Arabia

² Biosystems and Machines Interdisciplinary Research Center, King Fahd University of Petroleum and Minerals (KFUPM), Dhahran 31261, Saudi Arabia

³ Department of Computer Engineering, École Polytechnique Montréal, 2900 Edouard-Montpetit Boul, Montréal, QC H3T1J4, Canada; yoan.ladini@polymtl.ca (Y.L.); golriz.hosseinimanesh@polymtlus.ca (G.H.); imane.chafi@polymtlus.ca (I.C.); farida.cheriet@polymtl.ca (F.C.)

⁴ Intellident Dentaire Inc., Bureau 540, 1310 av Greene, Westmont, QC H3Z2B2, Canada; info@kerenor.ca

* Correspondence: ammar.sheghri@kfupm.edu.sa (A.A.); francois.guibault@polymtl.ca (F.G.)

Abstract: During a crown generation procedure, dental technicians depend on commercial software to generate a margin line to define the design boundary for the crown. The margin line generation remains a non-reproducible, inconsistent, and challenging procedure. In this work, we propose to generate margin line points on prepared teeth meshes using adaptive point learning inspired by the AdaPointTr model. We extracted ground truth margin lines as point clouds from the prepared teeth and crown bottom meshes. The chamfer distance (CD) and infoCD loss functions were used for training a supervised deep learning model that outputs a margin line as a point cloud. To enhance the generation results, the deep learning model was trained based on three different resolutions of the target margin lines, which were used to back-propagate the losses. Five folds were trained and an ensemble model was constructed. The training and test sets contained 913 and 134 samples, respectively, covering all teeth positions. Intraoral scanning was used to collect all samples. Our post-processing involves removing outlier points based on local point density and principal component analysis (PCA) followed by a spline prediction. Comparing our final spline predictions with the ground truth margin line using CD, we achieved a median distance of 0.137 mm. The median Hausdorff distance was 0.242 mm. We also propose a novel confidence metric for uncertainty quantification of generated margin lines during deployment. The metric was defined based on the percentage of removed outliers during the post-processing stage. The proposed end-to-end framework helps dental professionals in generating and evaluating margin lines consistently. The findings underscore the potential of deep learning to revolutionize the detection and extraction of 3D landmarks, offering personalized and robust methods to meet the increasing demands for precision and efficiency in the medical field.

Keywords: dental margin line; point cloud generation; deep learning; uncertainty quantification



Citation: Alsheghri, A.; Ladini, Y.; Hosseinimanesh, G.; Chafi, I.; Keren, J.; Cheriet, F.; Guibault, F. Adaptive Point Learning with Uncertainty Quantification to Generate Margin Lines on Prepared Teeth. *Appl. Sci.* **2024**, *14*, 9486. <https://doi.org/10.3390/app14209486>

Academic Editor: Douglas O'Shaughnessy

Received: 19 September 2024

Revised: 9 October 2024

Accepted: 11 October 2024

Published: 17 October 2024



Copyright: © 2024 by the authors. Licensee MDPI, Basel, Switzerland. This article is an open access article distributed under the terms and conditions of the Creative Commons Attribution (CC BY) license (<https://creativecommons.org/licenses/by/4.0/>).

1. Introduction

Dental crown treatment is among the most common in dentistry to restore damaged or decayed teeth. Dental crowns are created through a process involving dental professionals and laboratories. Dentists examine and prepare teeth that need a crown treatment by reshaping the teeth, while removing diseased sections. The dentist then takes impressions of the prepared tooth, which can be performed using traditional methods or digital scanning. A die represents the prepared tooth of the patient needing a crown restoration. Crowns are then designed and produced in dental laboratories ensuring a precise fit and aesthetic appearance. In modern practice, dental technicians use computer software to design a

crown to sit on the scanned die. The digital crown design procedure has several steps with the most important one being the accurate detection of the margin line on the surface of the die [1]. In this work, we propose an automated and personalized deep learning framework to extract margin lines from dental preparations. The proposed framework incorporates a novel uncertainty quantification metric to provide confidence level of the predicted margin lines.

Margin lines constitute the boundaries of dental crowns. Current dental software use traditional search algorithms and optimization frameworks to detect appropriate margin lines that avoid undercuts. However, due to the huge variability in teeth among patients, the produced margin lines are not always precise [2]. Often, dental technicians need to manually intervene to correct margin lines before resuming the crown generation procedure, which constitutes an inconsistent and non repeatable step in the design process. The automated and accurate identification of margin lines on prepared teeth forms a bottleneck in the digital automation of dental restoration design [3].

The use of machine learning (ML) has been increasing in the field of digital dentistry [4–6]. Many problems in digital dentistry require personalized solutions that are difficult to automate using traditional computation methods. ML has the ability to learn from the huge amounts of available dental data to provide personalized solutions. ML has been used in prosthodontic-driven rehabilitation of patients [7], teeth classification [8,9], teeth segmentation [10–14], caries and cavities detection [15,16], arch registration [17], and crown generative tasks [18]. However, to the best of the authors' knowledge, there is a lack of research investigating the use of ML in detecting margin lines on dental preparations.

Geometric methods have been proposed to automatically detect margin lines [19]. However, they highly depend on the presence of sharp features at the margin line. Traditional geometric and optimization techniques based on curvatures may fail in certain regions where curvature features are missing. Deep learning (DL) could have an edge over traditional computer-aided design (CAD) techniques [20], particularly due to the huge variability in teeth shapes and the ability of DL to handle complex data.

The automation and successful identification of a margin line is considered as the most important procedure for automated crown generation in digital dentistry. Our contributions in this paper include the following: (1) We propose an end-to-end framework based on a transformer-based neural network for margin line generation on surfaces of prepared teeth. Different from existing approaches, we use multi-resolutions of the target data to train the DL model. In addition, the transformer-based network is used for point cloud generation whereas the focus of related work is on point cloud completion. Ensemble learning was also used to enhance the generated point cloud predictions. (2) A novel denoising post-processing algorithm is proposed to remove outliers and predict a spline representation of the margin line. (3) We propose a novel confidence metric for evaluating model uncertainty in real-time deployment. Because the ground truth is not unique, this offers a decision-support tool to auto-evaluate the model prediction. To the best of the authors' knowledge, the use of uncertainty metrics in the context of margin line generation has not been discussed in the literature.

The proposed uncertainty estimation helps in offsetting the lack of external supervision by helping the model become self-sufficient and interpretable. As such, it enhances the reliability and robustness of the model. Related work is presented in the next section, followed by methods, results, discussion, and conclusions. Table 1 lists the descriptions of most common abbreviations used in the paper.

Table 1. The most common abbreviations used in the paper.

Abbreviation	Description
AI	Artificial intelligence
ML	Machine learning
DL	Deep learning
PCA	Principal component analysis
UQ	Uncertainty quantification
CD	Chamfer distance
CAD	Computer-aided design
CAM	Computer-aided manufacturing
DGCNN	Deep graph convolutional neural network
GANs	Generative adversarial networks
LD	Local density
API	Application programming interface
HD	Hausdorff distance

2. Related Work

This section provides a concise review of margin line extraction, point cloud generation, and uncertainty quantification. The first sub-section provides a broader context of the use of CAD/CAM in digital dentistry.

2.1. CAD/CAM Systems in Digital Dentistry

Advanced CAD/CAM technologies are increasingly utilized in digital dentistry for several applications, including orthodontics [21,22], prosthodontics [23–25], and intraoral scanning [26]. Recent studies recommended that digitally designed crowns and bridges created by professional with experience in CAD/CAM and dental technology are likely to provide patients with anterior prosthetic rehabilitation a high level of satisfaction and comfort [27]. In addition, dental professionals are finding significant value in the design quality, convenience, and reproducibility offered by AI integration within CAD/CAM systems [28]. As mentioned in our introduction, AI is paving the way for automated and reproducible frameworks, particularly within CAD systems.

2.2. Margin Line Extraction

Despite significant advancements in digital dentistry, the issue of automating the extraction of a dental preparation margin line remains unresolved. Only a few works specifically addressed the task of margin line detection. Previous work improved the A* algorithm to produce a feature line with the help of two interactive points provided by the user [29]. Another work used the bidirectional path search to determine the margin line [30]. However, it presented certain limitations including the need of user input with no guarantee of a globally optimal solution. A segmentation DL model [31] was used by another group to extract the margin line. This method also presented limitations to deal with cases missing sharp features at the margin region. In a more recent study, the accuracy of a new hybrid method in extracting the margin line was compared with existing software programs [32]. The study concluded that using a hybrid method combining deep learning and CAD enables the robust and accurate extraction of margin lines. In the current work, we represent the margin line extraction problem as a point cloud generation problem where a point cloud of a die is provided, and the DL model should generate the points of the corresponding margin line.

2.3. Point Cloud Generation

Three-dimensional point cloud generation is a critical task in computer vision. Various DL models have been developed to tackle this problem, as comprehensively reviewed in [33]. Point-based methods, such as PointNet [34] and PointNet++ [35], directly process the raw 3D coordinates of point clouds and have shown significant promise due to their ability to handle unordered point sets and learn local and global features effectively. Convolution-based methods [36] apply 3D convolutions to voxelized representations of point clouds, benefiting from the regular grid structure of voxels but are computationally expensive and limited by resolution constraints. Graph-based methods [37] represent point clouds as graphs, leveraging graph neural networks to capture relational information between points, thus achieving more accurate completions. Generative model-based approaches, including generative adversarial networks (GANs) [38], generate plausible completions by modeling the underlying data distribution. Recent improvements have been made in the field of shape generation [39,40] and specifically in dentistry [1]. Conditional GANs were used for generating crowns that reduce the occlusal problems seen in restorations [41]. Recently, transformer-based architectures have been applied to point cloud generation tasks, adeptly capturing long-range dependencies within point clouds. Notable examples include ‘point transformer’, which uses self-attention mechanisms to learn interactions across long distances; PT2PC [42], which combines transformers with point cloud processing techniques for fine-grained completions; PoinTr [43], which employs a transformer encoder-decoder architecture to model global features for point cloud completion; and AdaPoinTr [44], which leverages transformer architectures with geometry-aware blocks and adaptive query generation for point cloud completion. Despite these advancements, challenges such as learning localized details from unstructured point clouds and generating fine-grained predictions remain.

2.4. Uncertainty Quantification (UQ) in Deep Learning (DL)

DL has been extensively used in medical applications for a variety of tasks including detection, segmentation, generation, and classification [45]. However, the lack of ground truth and issues with UQ remain unsolved. UQ in DL aims at understanding the uncertainty associated with the predictions made by the model [46]. Uncertainty can arise from various sources, including the model’s parameters, the data, and the inherent limitations of the model architecture itself. Researchers discussed two types of uncertainty: (i) epistemic, which captures the uncertainty of the model, and (ii) aleatoric, which captures the noise in the data [47]. Recent studies considered UQ in DL on 3D data for segmentation of point clouds [33,48], bounding box detection [49], and diffusion MRI [50]. Nevertheless, there exists a lack of studies to quantify uncertainty in point cloud generation problems to evaluate the reliability of the predicted point clouds.

3. Methods

3.1. Preprocessing Input Data

The proposed DL framework is based on a point cloud generation model that receives an intraoral die scan as an input and outputs a margin line as a point cloud first, and then a spline representation. Therefore, we first converted the input mesh to a point cloud and then decimated it to 10,000 points for enhanced computational speed and efficiency (Figure 1).

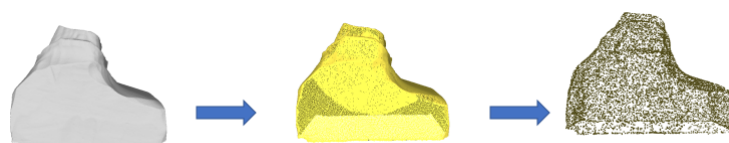


Figure 1. Converting die meshes to point clouds and downsampling the point clouds to 10,000 points.

3.2. Extracting Ground Truth Margin Lines

To generate the ground truth target margin lines, we needed as an input the die scan (which is also the input of the model during the inference stage) and the crown scan associated to it. The crown 3D models were previously designed by a dental professional (including the bottom band of the shell representing the thickness of the crown at the margin line region). We extracted the boundary band at the bottom of the crown and selected from it the closest points to the die. Then, we projected those points onto the die to ensure they intercept it. Finally, we augmented the projected points by creating a point in the middle of two neighbors until we reached at least 5000 points to represent the ground truth margin line (Figure 2).

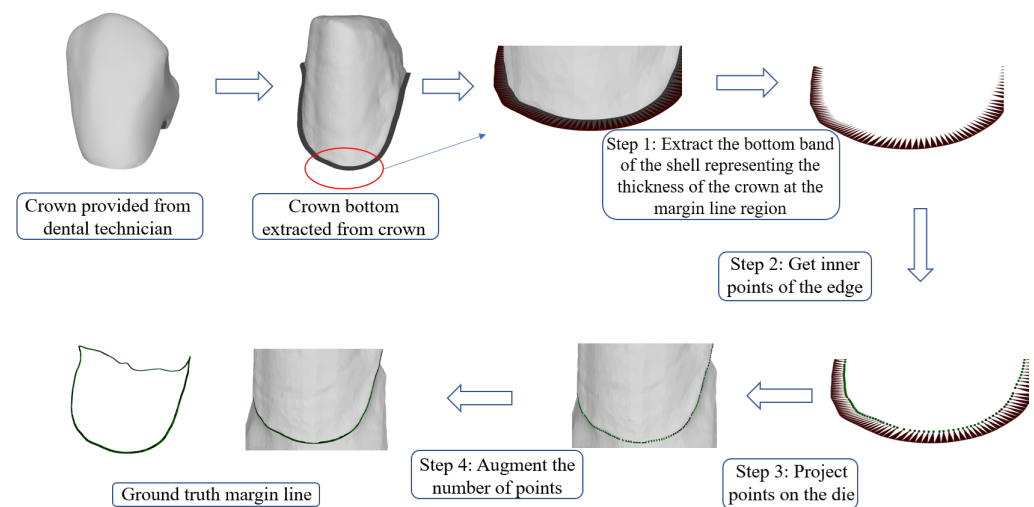


Figure 2. Extracting ground truth margin lines. A crown bottom is first extracted from a crown designed by a dental technician. The internal edge of crown bottom lower horizontal thickness coincides with the margin line on the dental preparation. The internal points are extracted, projected on the die, and augmented to represent the margin line.

3.3. Deep Learning Model

We based our model on the AdaPoinTr [44] architecture, which proved to be performing well in set-to-set point completion (Figure 3). The model takes as input a point cloud of the die with 10,000 points. It first uses the farthest point sampling technique (FPS) to obtain the center points of the input. FPS facilitates the grouping of the input point cloud into a smaller set of features to then be converted into a series of vectors and used by the transformer architecture. FPS provides a structured output of points while preserving the shape features in a computationally efficient manner making it suitable for real-time application [34]. A deep graph convolutional neural network (DGCNN) is then applied, which downsamples the input point cloud further by extracting the features of center points. This is necessary to reduce the complexity of the model. Afterwards we inject the N features in the encoder block, to obtain the feature vectors $V = V_1, V_2, \dots, V_N$ as an output. The output is injected to the adaptive query generator, which consists of a multilayer perceptron (MLP) making queries. Then, another MLP selects M queries from the previous output. As a result we obtain $Q = Q_1, Q_2, \dots, Q_M$. Those queries are injected in the first geometry-aware transformer block (self-attention block) from the decoder. Then, the output of the first block is injected with feature vector into the second block of the decoder (cross-attention block). The results provided by the decoder consist of point proxies. To provide a complete prediction, a Folding Net is then used to rebuild the point cloud from the point proxies and output both a coarse and a fine predictions (Figure 3).

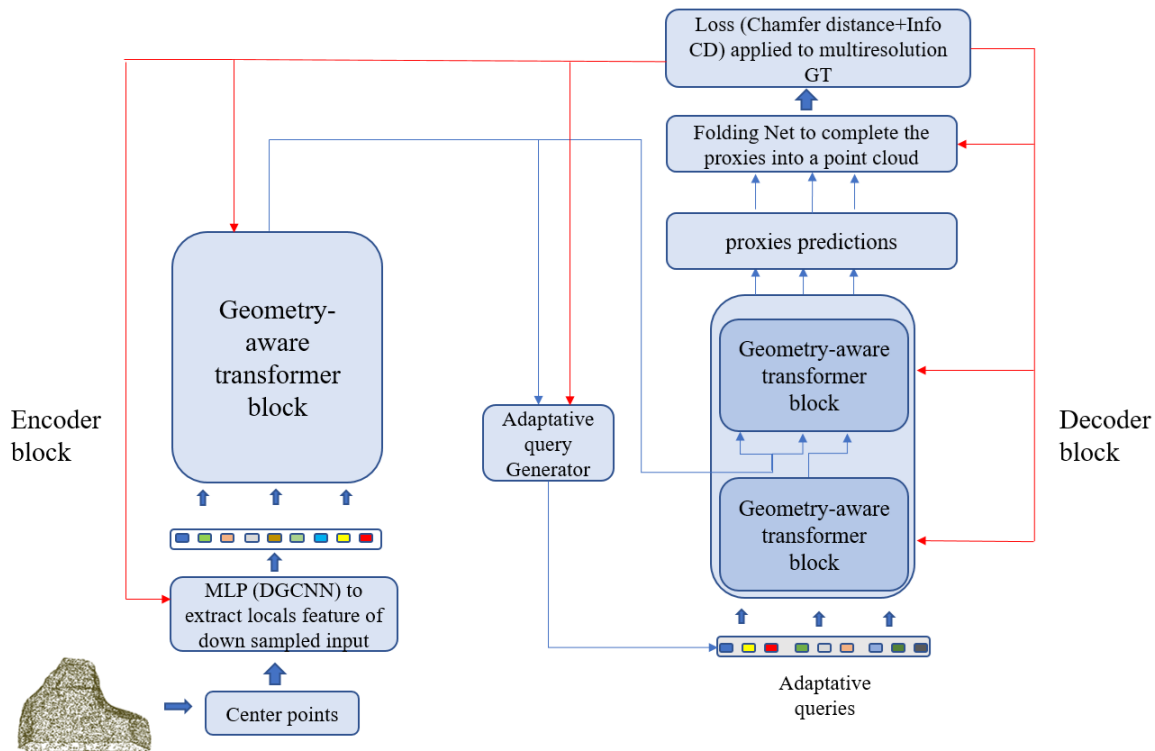


Figure 3. AdaPoinTr architecture showing the forward pass in blue arrows and backpropagation pass in red.

3.4. Metrics

The final prediction was evaluated with a combination of chamfer distance and infoCD applied on coarse ground truth to coarse prediction, medium ground truth to fine prediction, and fine ground truth to fine prediction. The loss obtained was retro-propagated to the folding net, the first and second blocks of the decoder, both MLPs inside the adaptive query generator, the encoder, and the DGCNN.

3.4.1. Chamfer Distance (CD)

The DL model generates two resolutions; fine and coarse. Both resolutions were used to back propagate the chamfer distance loss. We used two different versions of chamfer distance CD 1 and CD 2 for the training loss as defined by the following equations [51]:

$$\mathcal{L}_{CD}(a_i, b_i) = \ell_{CD}(a_i, b_i) + \ell_{CD}(b_i, a_i) = \frac{1}{|b_i|} \sum_k \min_j d(a_{ij}, b_{ik}) + \frac{1}{|a_i|} \sum_j \min_k d(a_{ij}, b_{ik}) \quad (1)$$

where $|\cdot|$ denotes the cardinality of a set and function d refers to

$$d(x_{ij}, y_{ik}) = \begin{cases} \|x_{ij} - y_{ik}\| & \text{as L1-distance} \\ \|x_{ij} - y_{ik}\|^2 & \text{as L2-distance} \end{cases} \quad (2)$$

where $\|\cdot\|$ denotes the Euclidean ℓ_2 norm of a vector.

While CD 1 aims to highlight robustness to outliers and is less concerned with penalizing small discrepancies heavily, CD 2 focuses on the precise alignment of shapes with a focus on penalizing minor discrepancies. The dimensional unit for CD 2 is mm^2 and for CD 1 is mm . Although both CD 1 and CD 2 were used for training, only CD 1 was used for the evaluation because CD 1 tends to focus more on penalizing outliers and it is easier to interpret compared with CD 2 due to its dimensional unit. In this paper, the term CD refers to CD 1 because it was the only one used during the evaluation.

3.4.2. Info CD

InfoCD is an improvement on contrastive chamfer distance loss. We chose to use InfoCD in training as a complement to chamfer distance as a state-of-the-art metric, following the implementation by [51]. InfoCD allows for the distribution of point clouds in alignment. This provides less sensitivity to outliers than a simple chamfer distance loss (CD). This is due to InfoCD maximizing the lower bound of the mutual information between geometric surfaces portrayed in point clouds [51]. As such, the InfoCD metric is efficient and robust for machine learning applications. The InfoCD loss used in training is defined based on the work of [51] as follows:

$$\mathcal{L}_{\text{InfoCD}}(a_i, b_i) = \ell_{\text{InfoCD}}(a_i, b_i) + \ell_{\text{InfoCD}}(b_i, a_i) \quad (3)$$

$$\ell_{\text{InfoCD}}(a_i, b_i) = -\frac{1}{|b_i|} \sum_k \log \left\{ \frac{\exp \left\{ -\frac{1}{2} \min_j d(a_{ij}, b_{ik}) \right\}}{\sum_k \exp \left\{ -\frac{1}{2} \min_j d(a_{ij}, b_{ik}) \right\}} \right\} \quad (4)$$

where (a_i, b_i) are the i -th point pair from two different point clouds, $d(.,.)$ is a distance equation as L1 distance.

3.4.3. Hausdorff Distance (HD)

The HD is another metric used to measure the similarity between two point clouds [52,53]. It helps quantify how far two point clouds are from each other. However, it is considered more strict compared with CD because it measures the maximum distance from a point in one set to the closest point in the other set. This means it focuses on the most distant outliers. The Hausdorff distance D_H between two sets of points X and Y is calculated using the following equations:

$$D_H(X, Y) = \max(d_H(X, Y), d_H(Y, X)) \quad (5)$$

$$d_H(X, Y) = \max_{x \in X} \left(\min_{y \in Y} \|x - y\| \right) \quad (6)$$

3.4.4. Confidence Metric

The DL model generates a prediction as a point cloud that may not necessarily form a unique closed curve. It can also occur that the prediction does not look like a curve for some difficult cases where it is challenging to determine a precise margin line even with the human eye (Figure A1). To make our model viable for real use cases in deployment, there is a need to evaluate the output and quantify uncertainty without ground truth. The confidence of a margin line prediction could be measured using a confidence metric. In this work, we propose an efficient technique to detect outliers, and based on the percentage of identified outliers, a boolean confidence metric was proposed for the model prediction. Outliers detection is detailed later in the post-processing section.

3.4.5. Confidence Metric Versus CD Evaluation

To measure the correlation of our confidence metric with CD, we compared the results provided by CD (a value greater than 0.2 is considered actual non-confident) with the confidence metric results (more than 0.65% outliers detected is considered predicted non-confident). The 0.2 mm threshold for CD was selected based on a study that investigated the accuracy of manual margin line detection and reported errors that reached up to 0.210 mm using EXOCAD (DentalCAD 3.0 Galway; EXOCAD GmbH, Darmstadt, Germany) and 0.215 mm using R2CAD software (MegaGen; Daegu, South Korea) [2]. The threshold of 0.65% for outliers was established based on qualitative observations and frequency distribution of CD and percentage of outliers for the validation and test sets. Histograms were established for the frequency versus CD and frequency versus percentage of outliers

for the five folds of the models with both the test and validation sets. On average, the frequency of data corresponding to a CD value of 0.2 corresponded to a threshold of 0.65% for outliers. Figure A2 shows representative histograms for fold 2 from the test set.

Table 2 shows the confusion matrix. A true positive (TP) measure corresponds to $CD < 0.2$ and outliers $< 0.65\%$. A true negative (TR) corresponds to $CD \geq 0.2$ and outliers $\geq 0.65\%$. On the other hand, a false positive (FP) corresponds to $CD \geq 0.2$ and outliers $< 0.65\%$. A false negative (FN) corresponds to $CD < 0.2$ and outliers $\geq 0.65\%$. The accuracy, sensitivity, and precision metrics [54–56] were used to evaluate the correlations between the confidence metric and CD.

Table 2. Confusion matrix for correlations of CD with the proposed confidence metric.

Confusion Matrix CD versus Confidence Metric		Predicted Confidence Metric	
		Predicted Positive (Outliers $< 0.65\%$)	Predicted Negative (Outliers $\geq 0.65\%$)
Actual CD	Positive ($CD < 0.2$)	TP	FN
	Negative ($CD \geq 0.2$)	FP	TN

3.5. Training Details

Supervised training was used to train the model. The training set contained 913 samples augmented 20 times with a 80/20 split for training and validation. The test set included 134 samples. Our data, i.e., die scans, comes from 20 different dental clinics. The margin line extraction and crown design were achieved by two different dental technicians. To augment the training set, we used 20 different randomly generated augmentation matrices per case to change orientation, position (translation over x , y or z axis), and scale (stretch or expand over the axis it is applied to). The augmentation ranges were $[-180, 180]$ degrees for rotation over the z axis, $[-1, 1]$ for translation for all axes, and $[0.9, 1.1]$ scaling for all axes. Because our dataset is orientated towards the z axis, we limited rotations around the x and y axes to $[-30, 30]$ degrees to avoid flipping the die completely. Figure 4 shows an example of a training case augmented 20 times.

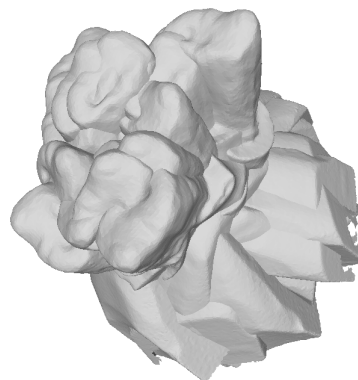


Figure 4. One case augmented 20 times.

A batch size of 8 was used to train the AdaPoinTr model with an output resolution of 1536 points. The AdamW optimizer was used with a weight decay of 0.0005 and a learning rate of 0.0001 combined with a lambda scheduler triggered every 21 epochs with a decay coefficient of 0.9 and a minimum value for learning rate of 0.000002. We used a batch normalization scheduler that triggers every 21 steps as well with decay coefficient of 0.5 on the moving average, a high momentum of 0.9, and the lowest value possible for a moving average as 0.01 of its initial value.

Training was conducted using a cluster with GPU NVIDIA A100-SXM4-40GB, 32 GB of RAM allocated and six CPU cores over three days (no limit on epochs). The loss converged after approximately 60 epochs for training and 70 epochs for validation (Figure A3). The

model of the last epoch was chosen as the best model to avoid overfitting. For the loss, we used a linear combination of CD and normalized infoCD. The value of infoCD was multiplied by 10^{-4} . The combined loss was used to adjust the gradients for backpropagation during the training. Five models were trained and validation set was varied among them.

3.6. Post-Processing

3.6.1. Ordering Point Cloud

To make a spline representation of the margin line, the point cloud should be ordered, which is not the case when the model produces an output. The travel sales person method was used to order the point cloud based on the Trimesh python library using the function `trimesh.points.tsp()`. This function selects an arbitrary starting point p_0 , then seeks the closest point p_1 using the shortest euclidean distance, and continues until visiting the whole set of points to finally return to p_0 . With this technique, some points that are not close enough to a neighbor might not be visited until the algorithm has made a complete lap of the margin line. Such points would be added at the end just before revisiting p_0 (Figure A4).

To overcome the ordering issue within our computational complexity (more than 1500 points), we investigated any anomalies in the last 10% of points and replaced them with new points interpolated between the two neighbors they are supposed to have. To identify an anomaly at a point p_i , we checked whether the distance to the previous neighbor $\text{dist}(p_i, p_{i-1})$ is abnormally long (more than three times the mean distance from one point to its neighbor) and its distance to p_0 , $\text{dist}(p_i, p_0)$ is shorter than the distance of its previous neighbor to p_0 , $\text{dist}(p_{i-1}, p_0)$. The set of points being anomalies can be defined as follows:

$$P_i \in \left((\text{dist}(P_i, P_{i-1}) > 3 \cdot \bar{d}) \cap \left(i > n - \frac{n}{10} \right) \cap (\text{dist}(P_i, P_0) > \text{dist}(P_{i-1}, P_0)) \right) \quad (7)$$

3.6.2. Spline

Once our point cloud is ordered, a B-spline is generated using the `scipy.interpolate.splprep()` function from Scipy python library. This function receives a point cloud and a smoothness factor and returns the B-spline parameters (knot vectors, control points, and degree of spline). Because a high precision is required, we chose a small smoothness factor of 0.015 based on qualitative observation of the results.

3.6.3. Removing Outliers

Before the prediction of spline parameters, it was necessary to remove outliers from the predicted point cloud to obtain smooth and precise splines. Our novel post-processing was based on local density and first component of principal component analysis (PCA). To evaluate if a point is an outlier [57], first we calculate the average distance \bar{d}_i for each point p_i based on its Euclidian distances with its k nearest neighbors $q_j (j = 1 \dots, k)$ such as:

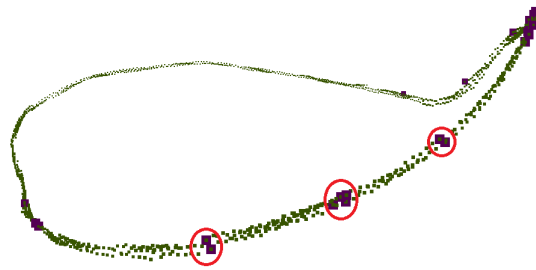
$$\bar{d}_i = \frac{1}{k} \sum_{j=1}^k \text{dist}(p_i, q_j) \quad (8)$$

Then we calculate the local density LD of p_i defined as:

$$LD(p_i) = \frac{1}{k} \sum_{q_j \in KNN(p_i)} \exp\left(-\frac{\text{dist}(p_i, q_j)}{\bar{d}_i}\right) \quad (9)$$

where KNN is the k nearest neighbors of p_i . Then, from the observation of LD for each case, we define a threshold $\epsilon = 0.4$ to flag every point p_i with LD inferior to ϵ as an outlier. We decided to take $k = 50$ in our analysis. The parameters for ϵ and k were chosen by qualitative observation. For example, we observed that when the LD value for a point was below 0.4, this point would be isolated.

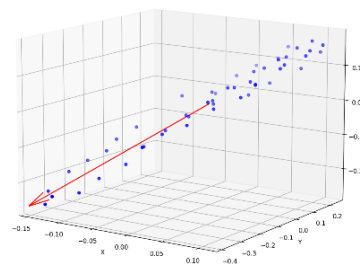
Using the local density calculations alone, another problem could arise when the predicted point cloud has some gaps. Some points will be identified as outliers because they do not have enough neighbors while they are not outliers in reality (Figure 5). To overcome this issue, we proposed to check whether a point p_i identified as an outlier follows the tendency of its neighborhood ($k = 50$). We used PCA first component to determine tendency (Figure 5), and made a projection p'_i of p_i to the tendency ray. If the distance $\text{dist}(p_i, p'_i)$ is greater than a relative threshold of 0.1, then p_i is considered an outlier. The post-processing process is illustrated in Figure 6.



(a) Outliers identifications with local density alone.



(b) Outliers identifications with local density and PCA.



(c) PCA first component.

Figure 5. Identifying outliers with (a) local density only; (b) with local density and PCA; (c) first component of PCA. Purple represents outliers in (a,b). With both local density and PCA, less outliers are observed.

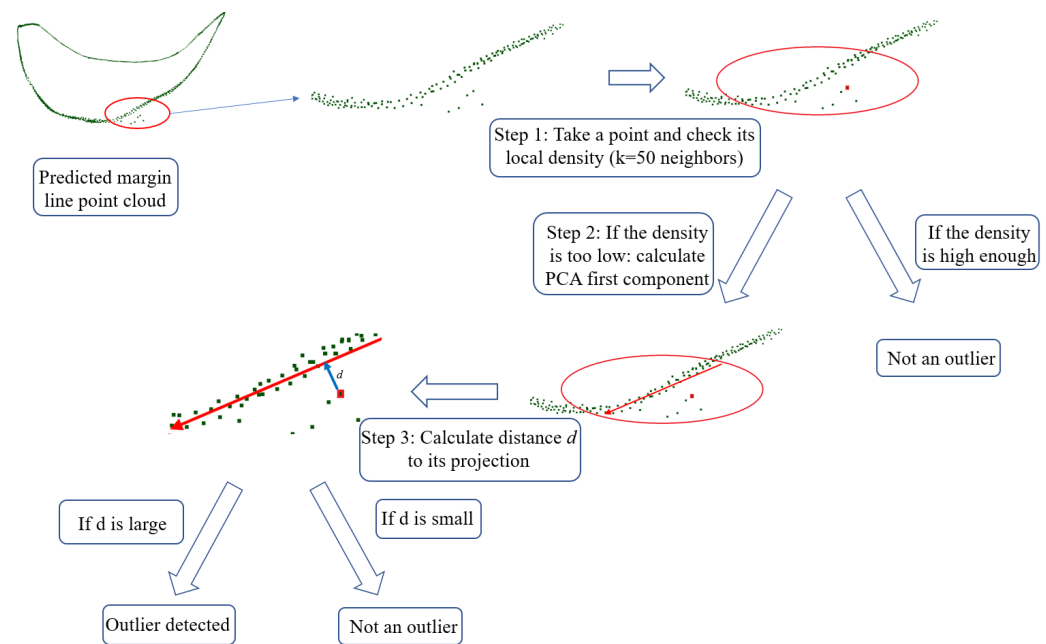


Figure 6. Illustration of the post-processing procedures to remove outliers.

4. Results

4.1. Prediction of Margin Lines

Table 3 shows the overall accuracy of the five folds reported in terms of the chamfer distance L1 norm (CD). CD was reported for the raw prediction of the margin line point cloud before removing outliers and for the spline fitted on the point cloud after removing outliers. The percentage of outliers is also presented in the table. According to the Shapiro–Wilk test, the results for the percentage of outliers and CD are not normally distributed. Therefore, we reported the median values in the table. In addition to the five individual folds, we reported the results obtained by their combination (i.e., best of five folds) as shown in the table. This combined result was obtained by identifying the model with the least percentage of outliers for each case, and selecting it to provide the point cloud of the margin line for that case.

As shown in Table 3, the individual models trained with the five folds yielded different results for CD of the raw predictions ranging from 0.121 to 0.134, and the splines ranging from 0.139 to 0.151. The CD values for splines were higher than raw predictions of point clouds for all models. It was also observed that the model with the minimum CD for raw prediction (i.e., fold 2), scored also the least for spline CD. The model with the minimum percentage of outliers (i.e., fold 4) did not provide the least CD neither for raw predictions nor for splines. It is also observed that the combined model (i.e., best of five folds) scored the minimum CD for splines compared with all individual folds. This is also true for the percentage of outliers, except for fold 4 which had also no outliers.

Table 3. Median values of: (1) CD and HD of raw point cloud predictions and splines; (2) the percentage of outliers and confident predictions for five folds and combined model.

	Fold 1	Fold 2	Fold 3	Fold 4	Fold 5	Best of 5 Folds
Raw prediction CD [mm]	0.134	0.121	0.132	0.129	0.134	0.126
Spline CD [mm]	0.151	0.139	0.149	0.147	0.146	0.137
Raw prediction HD [mm]	0.327	0.268	0.301	0.277	0.304	0.260
Spline HD [mm]	0.276	0.233	0.266	0.249	0.263	0.242
Percentage of outliers [%]	0.130	0.130	0.065	0	0.065	0
Percentage of confident predictions [%]	68.66%	73.88%	76.12%	79.85%	73.13%	88.81%

4.2. Uncertainty Quantification (UQ)

Figure 7 shows the point cloud raw prediction of margin lines for four test cases at different positions (It is important to note that we are following the FDI World Dental Federation (ISO) notation for teeth numbering). It is observed that at regions where predictions match the ground truth, the output point cloud is dense whereas at regions where there are discrepancies, the output point cloud is sparse and far from the actual ground truth. Based on this inherent characteristic of the AdaPoinTr network, a confidence metric was synthesized to quantify uncertainty by identifying outliers based on local density and PCA.

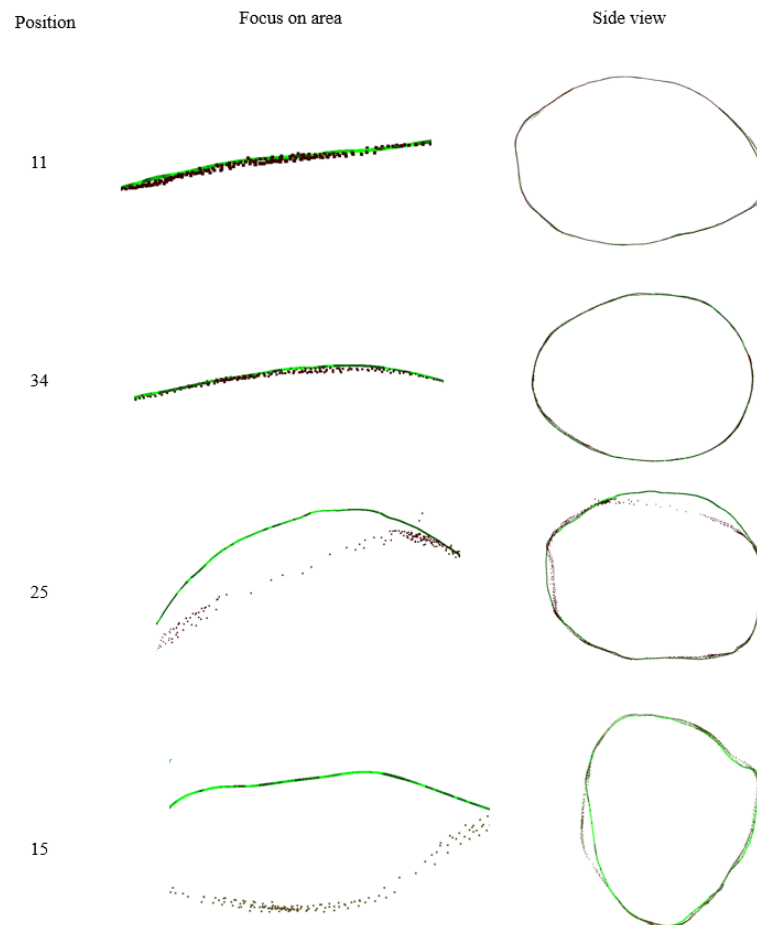


Figure 7. Predicted margin line point clouds of four test cases of different positions compared with ground truth. Red is the prediction, green is the ground truth.

Table 4 shows the correlations between the supervised metric CD and the proposed confidence metric for the five individual folds and the combined model created based on the unseen test set. The correlations were presented in terms of accuracy, sensitivity, and precision. The combined model was postulated based on voting among the models of the five folds. If three or more models voted as not confident, the combined model is not confident. It is observed in the table that no model could be classified as the best for all the different metrics simultaneously. The table also demonstrates that all models provided sensitivity and precision around 90% with averages of $91.92\% \pm 3.00\%$ and $91.64\% \pm 2.55\%$, respectively. Interestingly, the combined model provided scores close to average of the five individual models for all the metrics. The accuracy for all models was between 80% and 90% with an average of $87.76\% \pm 2.34\%$. Table 5 presents the correlations between CD and the confidence metric for the five folds based on the validation set. In general, the correlation metrics of all folds were lower for the validation set compared with the test

set. The average values obtained on the validation sets were $81.03\% \pm 2.11\%$ for accuracy, $86.79\% \pm 5.84\%$ for sensitivity, and $88.09\% \pm 3.58\%$ for precision.

Table 4. Correlations between confidence metric and CD for five individual folds and combined model on the unseen test set.

CD versus Confidence Metric	Fold 1	Fold 2	Fold 3	Fold 4	Fold 5	Combined
Accuracy	88.81	88.81	88.81	88.81	83.58	86.57
Sensitivity	89.69	91.18	93.94	96.00	88.78	92.08
Precision	94.57	93.94	91.18	89.72	88.78	90.29

Table 5. Correlations between confidence metric and CD for five individual folds on the validation sets.

CD versus Confidence Metric	Fold 1	Fold 2	Fold 3	Fold 4	Fold 5
Accuracy	81.97	79.78	80.77	84.07	78.57
Sensitivity	84.62	80.15	92.54	93.62	83.94
Precision	91.67	91.60	83.22	86.84	87.12

4.3. Effect of Outliers Removal

Figure 8 shows outliers in the raw predictions of four test cases (two anterior and two posterior). It also demonstrates the effect of removing outliers on the predicted splines for these cases. The model trained with fold 2 was selected to provide the predictions. For the four test cases, the predicted splines after removing outliers look closer to the ground truth margin lines shown in the figure compared with the splines before removing outliers. The confidence metric and CD are also presented for each test case. The CD values were reported by comparing the spline after removing outliers with the ground truth, whereas the confidence metric was reported based on the percentage of outliers without information about the ground truth margin lines. With a few number of isolated outliers as for cases of positions 11 and 26, the CD values were relatively small (i.e., smaller than the median of 0.139), and the predictions were confident according to the proposed confidence metric. The CD for test case of position 12 was relatively high (i.e., $0.210 > 0.139$). However, the predicted spline was similar to the ground truth margin line and the confidence metric yielded confident as shown in Figure 8. The prediction of the last test case of position 25 showed a wider region of outliers, which resulted in a higher CD and a non-confident prediction.

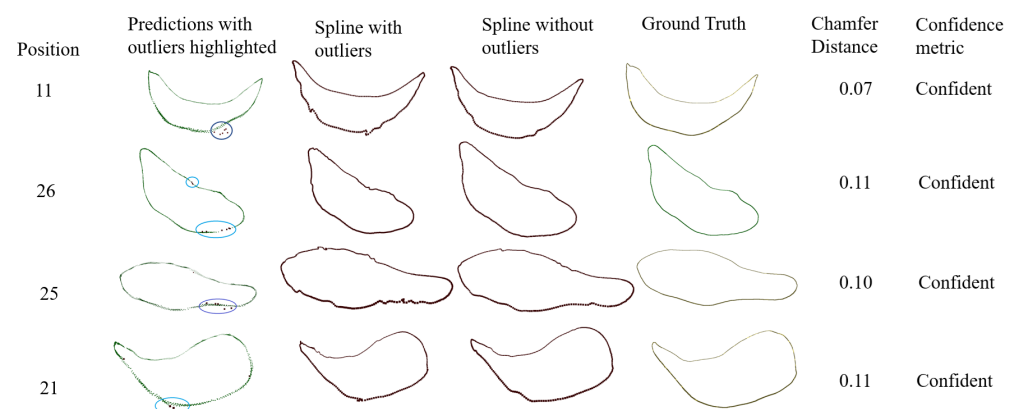


Figure 8. Qualitative comparison of margin lines obtained using the proposed framework showing the predicted points with outliers highlighted, the predicted margin line splines with outliers (baseline), the predicted splines without outliers improvement, and the ground truth margin lines. The chamfer distance and confidence metric are also presented for each test case.

4.4. Overall Qualitative and Quantitative Evaluation

Figure 9 shows the overall qualitative and quantitative efficiencies of the proposed framework for a variety of test cases spanning various teeth positions. For all the presented cases, the figure shows clear correspondences between margin line prediction as a spline after removing outliers and the ground truth margin lines. Most of the presented cases demonstrate low values of CD with a confident prediction. Cases with irregular shapes, as the one presented for position 27, showed a high value for CD and a non-confident prediction. In terms of other evaluations metrics, Table 3 reports median values of HD for the raw predictions and splines representing the margin lines. As shown in the table, HD is more strict than CD because it focuses on extreme points and is more sensitive to outliers.

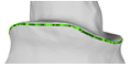

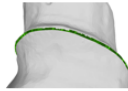
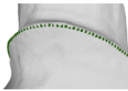
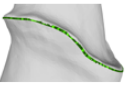
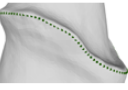


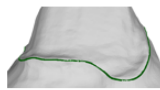
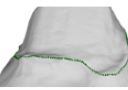



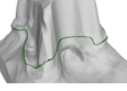
	Ground Truth	Ours	Chamfer Distance	Confidence metric
Position				
21			0.07	Confident
35			0.06	Confident
45			0.04	Confident
34			0.06	Confident
46			0.10	Confident
41			0.10	Confident
27			0.68	Non-Confident

Figure 9. Qualitative and quantitative results comparing the margin line predictions using our proposed model with the ground truth.

4.5. Example of a Challenging Case

A test case of position 34 is presented in Figure 10. When compared to the ground truth, the reported CD for this case was 0.792, based on fold 2. This may indicate that our algorithm failed to predict the margin line. However, the confidence metric returned a confident prediction based on the presence of only four outliers. As such, this case represents a false positive. Nevertheless, based on the opinion of a dental expert, there could be more than one solution to the margin line in such challenging cases due to the presence of two possible paths with high curvatures. Therefore, the predicted margin line could be considered as correct for this case.

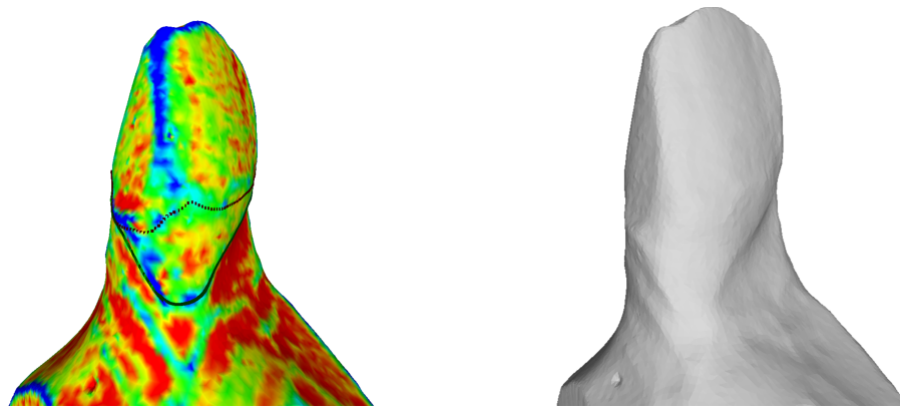


Figure 10. Challenging test case showing margin line prediction (dotted) compared with ground truth (solid), both overlaid on the die. The contours of the mean curvatures values of the die mesh are shown. Blue represents high curvature and red represents low curvature. The die geometry is also shown without contours.

5. Discussion

Our analysis and results confirm the possibility of predicting margin lines on the surfaces of prepared teeth. We propose an end-to-end framework to automatically generate accurate margin lines in the form of point clouds ($CD = 0.126$, $HD = 0.260$) or splines ($CD = 0.137$, $HD = 0.242$). This includes a post-processing procedure to remove outliers, which enhances the accuracy of the results. The predicted splines without outliers were closer to the ground truth showing the effectiveness of the proposed post-processing algorithm to remove noise and produce better margin lines (Figure 8). Furthermore, the implementation of five-fold cross-validation demonstrated the reliability and generalizability of the proposed deep learning framework (Table 3).

Our methodology to generate margin lines depends on a transformer model with adaptive query generation and denoising to generate the points representing the margin line. Previous related work in the literature depended on geometric optimization that requires initial point selection by the user [19] or segmentation techniques with a limited dataset [31]. Nevertheless, these approaches did not provide distance measures to quantitatively compare predicted and ground truth margin lines. Only recent work by Choi et al. reported distance measures [32]. The reported HD values by all of our five folds were less than the threshold of 0.566 mm reported by Choi et al. [32]. In terms of CD, Choi et al. reported CD L2 values whereas in our analysis we reported CD L1 because it has a unit of mm, which is more interpretable than CD L2 that has a unit of mm^2 . For the purpose of comparison, our CD L2 calculations reported a median value of 0.009 for spline predictions, which is less than the threshold reported by Choi et al. (i.e., 0.1). In addition, our framework is fully automated, which distinguishes it from Dentbird hybrid framework tested by [32]. Additionally, we propose a novel confidence metric as a tool aimed to provide feedback to users during deployment of the trained model. The confidence metric aids dental professional by indicating whether to trust generated margin lines without ground truth. Although, it could be treated as a percentage, we present it in this work as a boolean metric for simplicity. By estimating the confidence of the generated point cloud, we provide an UQ tool that can handle noise and outliers in the predictions. Different from previous studies that used the loss function [47] or sensitivity analysis [58] to quantify uncertainty, we used the direct output of the model to quantify outliers and evaluate uncertainty. Furthermore, the combination of UQ with ensemble learning resulted in 88.81% of confident predictions—higher than any of the individual trained folds (Table 3). This also highlights the efficiency of the ensemble model to make better predictions compared with individual folds.

While previous work presented confidence scores for point clouds in unsupervised registration [59] and object detection [60] tasks, to the best of the authors' knowledge, no

work has discussed confidence metrics for transformer-based point cloud generation. We correlated the newly proposed confidence metric with the CD metric based on the validation and test sets. The implemented five-fold cross-validation reflected the reliability of the correlation as shown in Tables 4 and 5. It is very critical to avoid false positive predictions where the model could trust a produced margin line that should not be considered correct. As such, the precision metric, which was around 90% on average between the validation and test sets, is considered critical in our case. On the other hand, it will not be dangerous if our model predicts a non-confident score for a good margin line. In other words, minimizing the false negative is not as important as minimizing the false positive. The slight deviation between the confidence metric and CD is because we established the confidence metric based on a strict boolean. Thresholds could be controlled by end users to be more or less conservative. In addition, the correlation metric values for the validation set (Table 5) were slightly lower than the test set (Table 4) due to the presence of more difficult cases in the validation set. In addition, the number of cases in the test set (i.e., 134) was lower than the validation set (i.e., 183).

The ablation study presented in Figure 8 demonstrated the effect of our novel technique of outlier removal on the final prediction of the margin line. Compared to the baseline model, which predicted a spline without removing outliers, the spline prediction after removing outliers showed a significant improvement. The spline prediction, representing the margin line, aligned more closely with the ground truth after the removal of outliers. Our five-fold cross-validation also showed consistent low values of the percentages of outliers identified as shown in Table 3 with all values being equal to or less than 0.13%.

Despite the advancement reported in the current study, it has some limitations. The first one is related to the time needed to obtain a prediction using the combined model, which is five times higher than a single model. The approximate time to generate a prediction, remove outliers, and turn it into a spline from one input is around 17 s. This includes 9 s to load the model and data, 6 s to remove outliers, and 2 s to make a spline. This time could be reduced using a multi-threading technique during deployment, which is currently in progress. Overall, the model accuracy and efficiency are expected to improve by training on a larger and more diverse dataset. The solution proposed is aimed to assist dental technicians in extracting the margin line. We decided to output the spline as a point cloud but also as a .json file containing the parameters of the spline. As such, this tool could be integrated into an API with a user interface that allows the user to move the control points of the spline to make modification easily and adjust the margin line if needed. In addition, the margin line extraction tool will be integrated with a crown generation deployed at <https://app.intellidentai.com/> Intellident (intellidentai.com).

Future work should consider the integration of the confidence metric in the loss function during training and the effect of that on the model accuracy and efficiency. In addition, methods of continuous learning based on expert feedback during deployment should be investigated. Recent strides have been made in the application of deep reinforcement learning in medical and dental imaging [61–63]. Future work can focus on integrating reinforcement learning such that feedback from deployment could be used to enhance the predictions of the model. Comparing the proposed confidence metric with alternative uncertainty quantification techniques should also be explored. Finally, we expect that implementing more sophisticated augmentation techniques will improve the model performance on challenging cases such as the ones presented in Figures 10 and A1. Examples of additional augmentations include die cropping, geometrical transformation, introducing random surface noise, and point dropping.

6. Conclusions

This study presented an accurate end-to-end framework to generate margin lines automatically on the surfaces of prepared teeth using deep learning. Our study contributes to state-of-the-art improvements in digital dentistry by providing a method to enhance digital restoration design. For the first time, we proposed a confidence metric on the

generated point clouds to provide uncertainty quantification of the margin line predictions in real-time deployment. To validate the reliability of the proposed framework, cross-validation was used by training five different folds of the deep learning model and ensuring consistent results for the chamfer distance (CD) and percentage of outliers. We also used ensemble learning to enhance the prediction of the framework by combining the results of the five folds. As a result, the obtained median CD on the test cases was 0.137 mm, the median HD was 0.242 mm, and percentage of confident predictions was increased to 88.81%. Future work should involve more data for training and testing, real-time deployment in dental laboratories, and development of a reinforcement learning algorithm to integrate professional feedback into the proposed framework.

Author Contributions: Conceptualization, A.A., F.G. and Y.L.; methodology, A.A. and Y.L.; software, Y.L., J.K., and F.G.; validation, A.A., J.K. and F.C.; formal analysis, A.A. and Y.L.; investigation, F.G. and F.C.; resources, F.G. and J.K.; data curation, J.K.; writing—original draft preparation, A.A., Y.L., G.H. and I.C.; writing—review and editing, A.A., F.G., F.C. and J.K.; visualization, Y.L. and A.A.; supervision, F.G. and F.C.; project administration, F.G.; funding acquisition, F.G. and A.A. All authors have read and agreed to the published version of the manuscript.

Funding: This work was funded by KerenOr, Intellident Dentaire Inc., iMD Research, the Natural Science and Engineering Research Council of Canada [Ref: ALLRP 583415-23], Institut de valorisation de données (IVADO) [Ref: PostDoc-2020a-5943530233], MEDTEQ [19-D Volumétrie dentaire 2], and King Fahd University of Petroleum and Minerals (KFUPM) [Ref: ISP23205].

Institutional Review Board Statement: The study was conducted according to the guidelines of the Declaration of Helsinki, and approved by the Polytechnique Montréal Research Ethics Committee (protocol code CER-2021-20-D, 29 September 2020).

Informed Consent Statement: Informed consent was obtained from all subjects involved in the study.

Data Availability Statement: The data underlying this article cannot be shared publicly to protect the privacy of individuals that participated in the study. We plan to deploy our model online at <https://app.intellidentai.com/> Intellident ([intellidentai.com](https://app.intellidentai.com/)).

Acknowledgments: We thank the Canadian Digital Alliance for providing the computational resources used in this work. The authors acknowledge the help and support from JACOB and Comet Technologies Canada Inc.

Conflicts of Interest: Author Julia Keren is employed at the companies KerenOr and Intellident Dentaire Inc. Author Ammar Alsheghri was employed by Comet Technologies Canada Inc. All authors declare that the research was conducted in the absence of any commercial or financial relationships that could be construed as a potential conflict of interest.

Appendix A



Figure A1. Worst margin line point cloud prediction recorded on a test case considered as a special case.

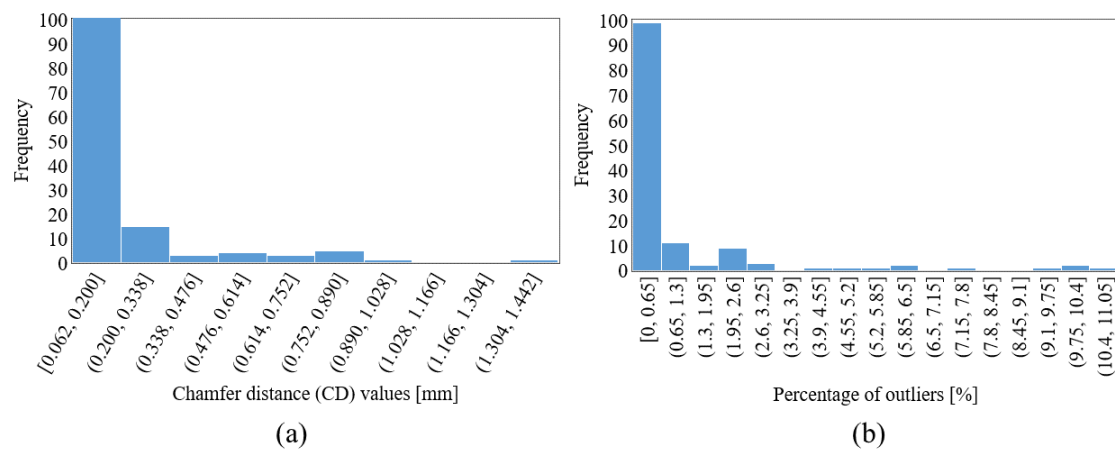


Figure A2. Representative frequencies of (a) CD values; (b) percentage of outliers, for the test set obtained using fold 2 model. CD values start from 0.062 mm because the prediction never matches the ground truth exactly.

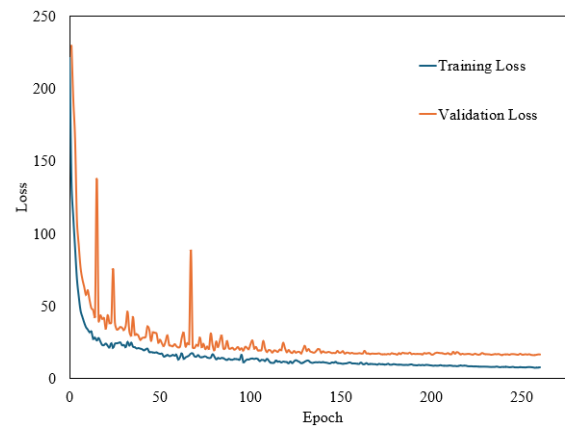


Figure A3. Representative CD training and validation loss curves.

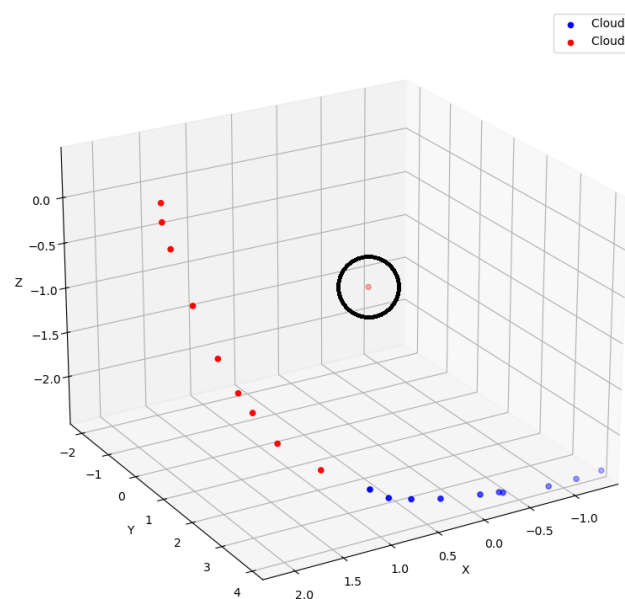


Figure A4. Ordering point cloud using travel sales person algorithm. The 10 lasts points of the point cloud are shown in red, and the first 10 are shown in blue. Notice that one red point is far from where it is supposed to be.

References

1. Chafi, I.; Cheriet, F.; Keren, J.; Zhang, Y.; Guibault, F. 3D generation of dental crown bottoms using context learning. In Proceedings of the Medical Imaging 2024: Imaging Informatics for Healthcare, Research, and Applications, San Diego, CA, USA, 18–22 February 2024; Volume 12931, pp. 98–104.
2. Mai, H.N.; Han, J.S.; Kim, H.S.; Park, Y.S.; Park, J.M.; Lee, D.H. Reliability of automatic finish line detection for tooth preparation in dental computer-aided software. *J. Prosthodont. Res.* **2023**, *67*, 138–143. [\[CrossRef\]](#)
3. Son, K.; Lee, K.B. Effect of finish line locations of tooth preparation on the accuracy of intraoral scanners. *Int. J. Comput. Dent.* **2021**, *24*, 29.
4. Revilla-León, M.; Gómez-Polo, M.; Vyas, S.; Barmak, A.B.; Özcan, M.; Att, W.; Krishnamurthy, V.R. Artificial intelligence applications in restorative dentistry: A systematic review. *J. Prosthet. Dent.* **2022**, *128*, 867–875. [\[CrossRef\]](#)
5. Carrillo-Perez, F.; Pecho, O.E.; Morales, J.C.; Paravina, R.D.; Della Bona, A.; Ghinea, R.; Pulgar, R.; Pérez, M.d.M.; Herrera, L.J. Applications of artificial intelligence in dentistry: A comprehensive review. *J. Esthet. Restor. Dent.* **2022**, *34*, 259–280. [\[CrossRef\]](#)
6. Piché, N.; Lasry, N.; Alsheghri, A.; Cheriet, F.; Ghadiri, F.; Guibault, F.; Hosseinimanesh, G.; Keren, J.; Lessard, O.; Zhang, Y.; et al. Automatic Generation of Dental Restorations Using Machine Learning, 2023. U.S. Patent App. 18/017,809, 7 September 2023.
7. Alshadidi, A.A.F.; Alshahrani, A.A.; Aldosari, L.I.N.; Chaturvedi, S.; Saini, R.S.; Hassan, S.A.B.; Cicciù, M.; Minervini, G. Investigation on the application of artificial intelligence in prosthodontics. *Appl. Sci.* **2023**, *13*, 5004. [\[CrossRef\]](#)
8. Chen, Q.; Huang, J.; Salehi, H.S.; Zhu, H.; Lian, L.; Lai, X.; Wei, K. Hierarchical CNN-based occlusal surface morphology analysis for classifying posterior tooth type using augmented images from 3D dental surface models. *Comput. Methods Programs Biomed.* **2021**, *208*, 106295. [\[CrossRef\]](#)
9. Alzubaidi, M.A.; Ootom, M. A comprehensive study on feature types for osteoporosis classification in dental panoramic radiographs. *Comput. Methods Programs Biomed.* **2020**, *188*, 105301. [\[CrossRef\]](#)
10. Tarce, M.; Zhou, Y.; Antonelli, A.; Becker, K. The Application of Artificial Intelligence for Tooth Segmentation in CBCT Images: A Systematic Review. *Appl. Sci.* **2024**, *14*, 6298. [\[CrossRef\]](#)
11. Alsheghri, A.; Ghadiri, F.; Zhang, Y.; Lessard, O.; Keren, J.; Cheriet, F.; Guibault, F. Semi-supervised segmentation of tooth from 3D scanned dental arches. In Proceedings of the Medical Imaging 2022: Image Processing, San Diego, CA, USA, 20–24 February 2022; Volume 12032, pp. 766–771.
12. Rubiu, G.; Bologna, M.; Cellina, M.; Cè, M.; Sala, D.; Pagani, R.; Mattavelli, E.; Fazzini, D.; Ibba, S.; Papa, S.; et al. Teeth segmentation in panoramic dental X-ray using mask regional convolutional neural network. *Appl. Sci.* **2023**, *13*, 7947. [\[CrossRef\]](#)
13. Wang, Y.; Xia, W.; Yan, Z.; Zhao, L.; Bian, X.; Liu, C.; Qi, Z.; Zhang, S.; Tang, Z. Root canal treatment planning by automatic tooth and root canal segmentation in dental CBCT with deep multi-task feature learning. *Med. Image Anal.* **2023**, *85*, 102750. [\[CrossRef\]](#)
14. Liao, J.; Wang, H.; Gu, H.; Cai, Y. PPA-SAM: Plug-and-Play Adversarial Segment Anything Model for 3D Tooth Segmentation. *Appl. Sci.* **2024**, *14*, 3259. [\[CrossRef\]](#)
15. Yoon, K.; Jeong, H.M.; Kim, J.W.; Park, J.H.; Choi, J. AI-based dental caries and tooth number detection in intraoral photos: Model development and performance evaluation. *J. Dent.* **2024**, *141*, 104821. [\[CrossRef\]](#)
16. Alharbi, S.S.; AlRugaibah, A.A.; Alhasson, H.F.; Khan, R.U. Detection of cavities from dental panoramic X-ray images using nested u-net models. *Appl. Sci.* **2023**, *13*, 12771. [\[CrossRef\]](#)
17. Kim, M.; Chung, M.; Shin, Y.G.; Kim, B. Automatic registration of dental CT and 3D scanned model using deep split jaw and surface curvature. *Comput. Methods Programs Biomed.* **2023**, *233*, 107467. [\[CrossRef\]](#)
18. Hosseinimanesh, G.; Ghadiri, F.; Alsheghri, A.; Zhang, Y.; Keren, J.; Cheriet, F.; Guibault, F. Improving the quality of dental crown using a transformer-based method. In Proceedings of the Medical Imaging 2023: Physics of Medical Imaging, San Diego, CA, USA, 19–23 February 2023; Volume 12463, pp. 802–809.
19. Han, S.; Yi, Y.; Revilla-León, M.; Yilmaz, B.; Yoon, H.I. Feasibility of software-based assessment for automated evaluation of tooth preparation for dental crown by using a computational geometric algorithm. *Sci. Rep.* **2023**, *13*, 11847. [\[CrossRef\]](#)
20. Mohammad-Rahimi, H.; Rokhshad, R.; Bencharit, S.; Krois, J.; Schwendicke, F. Deep learning: A primer for dentists and dental researchers. *J. Dent.* **2023**, *130*, 104430. [\[CrossRef\]](#)
21. Farah, R.I.; Alresheedi, B. Evaluation of the marginal and internal fit of CAD/CAM crowns designed using three different dental CAD programs: A 3-dimensional digital analysis study. *Clin. Oral Investig.* **2023**, *27*, 263–271. [\[CrossRef\]](#)
22. Ronsivalle, V.; Ruiz, F.; Lo Giudice, A.; Carli, E.; Venezia, P.; Isola, G.; Leonardi, R.; Mummolo, S. From reverse engineering software to CAD-CAM systems: How digital environment has influenced the clinical applications in modern dentistry and orthodontics. *Appl. Sci.* **2023**, *13*, 4986. [\[CrossRef\]](#)
23. Caron, E.; Marino, F.A.T.; Alageel, O.S.; Alsheghri, A.; Song, J. Computer-Aided Design and Manufacturing of Removable Partial Denture Frameworks with Enhanced Biomechanical Properties, 2021. U.S. Patent 10,959,818, 30 March 2021.
24. Richert, R.; Alsheghri, A.A.; Alageel, O.; Caron, E.; Song, J.; Ducret, M.; Tamimi, F. Analytical model of I-bar clasps for removable partial dentures. *Dent. Mater.* **2021**, *37*, 1066–1072. [\[CrossRef\]](#)
25. Alsheghri, A.A.; Alageel, O.; Caron, E.; Ciobanu, O.; Tamimi, F.; Song, J. An analytical model to design circumferential clasps for laser-sintered removable partial dentures. *Dent. Mater.* **2018**, *34*, 1474–1482. [\[CrossRef\]](#)
26. Revilla-León, M.; Kois, D.E.; Zeitler, J.M.; Att, W.; Kois, J.C. An overview of the digital occlusion technologies: Intraoral scanners, jaw tracking systems, and computerized occlusal analysis devices. *J. Esthet. Restor. Dent.* **2023**, *35*, 735–744. [\[CrossRef\]](#)

27. Cuschieri, L.A.; Casha, A.; No-Cortes, J.; Ferreira Lima, J.; Cortes, A.R.G. Patient satisfaction with anterior interim CAD-CAM rehabilitations designed by CAD technician versus trained dentist—A clinical preliminary study. *Appl. Sci.* **2023**, *13*, 8243. [\[CrossRef\]](#)
28. Son, K.; Kim, G.R.; Kim, W.G.; Kang, W.; Lee, D.H.; Kim, S.Y.; Lee, J.M.; Kim, Y.G.; Kim, J.W.; Lee, S.T.; et al. Requirements for Dental CAD Software: A Survey of Korean Dental Personnel. *Appl. Sci.* **2023**, *13*, 2803. [\[CrossRef\]](#)
29. Li, X.; Wang, X.; Chen, M. Accurate extraction of outermost biological characteristic curves in tooth preparations with fuzzy regions. *Comput. Biol. Med.* **2018**, *103*, 208–219. [\[CrossRef\]](#)
30. Shin, H.S.; Li, Z.; Kim, J.J. Feature extraction for margin lines using region growing with a dynamic weight function in a one-point bidirectional path search. *J. Comput. Des. Eng.* **2022**, *9*, 2332–2342. [\[CrossRef\]](#)
31. Zhang, B.; Dai, N.; Tian, S.; Yuan, F.; Yu, Q. The extraction method of tooth preparation margin line based on S-Octree CNN. *Int. J. Numer. Methods Biomed. Eng.* **2019**, *35*, e3241. [\[CrossRef\]](#)
32. Choi, J.; Ahn, J.; Park, J.M. Deep learning-based automated detection of the dental crown finish line: An accuracy study. *J. Prosthet. Dent.* **2023**, in press. [\[CrossRef\]](#)
33. Guo, Y.; Wang, H.; Hu, Q.; Liu, H.; Liu, L.; Bennamoun, M. Deep learning for 3d point clouds: A survey. *IEEE Trans. Pattern Anal. Mach. Intell.* **2020**, *43*, 4338–4364. [\[CrossRef\]](#)
34. Qi, C.R.; Su, H.; Mo, K.; Guibas, L.J. PointNet: Deep Learning on Point Sets for 3D Classification and Segmentation. In Proceedings of the IEEE Conference on Computer Vision and Pattern Recognition (CVPR), Honolulu, HI, USA, 21–26 July 2017; pp. 77–85.
35. Qi, C.R.; Yi, L.; Su, H.; Guibas, L.J. PointNet++: Deep Hierarchical Feature Learning on Point Sets in a Metric Space. *arXiv* **2017**, arXiv:cs.CV/1706.02413.
36. Hua, B.S.; Tran, M.K.; Yeung, S.K. Pointwise convolutional neural networks. In Proceedings of the IEEE Conference on Computer Vision and Pattern Recognition, Salt Lake City, UT, USA, 18–22 June 2018; pp. 984–993.
37. Wang, Y.; Sun, Y.; Liu, Z.; Sarma, S.E.; Bronstein, M.M.; Solomon, J.M. Dynamic graph cnn for learning on point clouds. *Acm Trans. Graph.* **2019**, *38*, 1–12. [\[CrossRef\]](#)
38. Goodfellow, I.; Pouget-Abadie, J.; Mirza, M.; Xu, B.; Warde-Farley, D.; Ozair, S.; Courville, A.; Bengio, Y. Generative adversarial nets. *Adv. Neural Inf. Process. Syst.* **2014**, *27*. [\[CrossRef\]](#)
39. Li, R.; Li, X.; Hui, K.H.; Fu, C.W. SP-GAN: Sphere-Guided 3D Shape Generation and Manipulation. *arXiv* **2021**, arXiv:2108.04476. [\[CrossRef\]](#)
40. Li, S.; Walder, C.J.; Liu, M. SPA-VAE: Similar-Parts-Assignment for Unsupervised 3D Point Cloud Generation. *arXiv* **2022**, arXiv:2203.07825.
41. Tian, S.; Wang, M.; Dai, N.; Ma, H.; Li, L.; Fiorenza, L.; Sun, Y.; Li, Y. DCPR-GAN: Dental Crown Prosthesis Restoration Using Two-Stage Generative Adversarial Networks. *IEEE J. Biomed. Health Inform.* **2022**, *26*, 151–160. [\[CrossRef\]](#)
42. Pan, X.; Xia, Z.; Song, S.; Li, L.E.; Huang, G. 3d object detection with pointformer. In Proceedings of the IEEE/CVF Conference on Computer Vision and Pattern Recognition, Nashville, TN, USA, 19–25 June 2021; pp. 7463–7472.
43. Yu, X.; Rao, Y.; Wang, Z.; Liu, Z.; Lu, J.; Zhou, J. Pointr: Diverse point cloud completion with geometry-aware transformers. In Proceedings of the IEEE/CVF International Conference on Computer Vision, Montreal, BC, Canada, 11–17 October 2021; pp. 12498–12507.
44. Yu, X.; Rao, Y.; Wang, Z.; Lu, J.; Zhou, J. AdaPoinTr: Diverse Point Cloud Completion with Adaptive Geometry-Aware Transformers. *arXiv* **2023**, arXiv:cs.CV/2301.04545. [\[CrossRef\]](#)
45. Chen, X.; Wang, X.; Zhang, K.; Fung, K.M.; Thai, T.C.; Moore, K.; Mannel, R.S.; Liu, H.; Zheng, B.; Qiu, Y. Recent advances and clinical applications of deep learning in medical image analysis. *Med. Image Anal.* **2022**, *79*, 102444. [\[CrossRef\]](#)
46. Huang, L.; Ruan, S.; Xing, Y.; Feng, M. A review of uncertainty quantification in medical image analysis: Probabilistic and non-probabilistic methods. *Med. Image Anal.* **2024**, *31*, 103223. [\[CrossRef\]](#)
47. Karthik, E.N.; Cheriet, F.; Laporte, C. Uncertainty estimation in unsupervised MR-CT synthesis of scoliotic spines. *IEEE Open J. Eng. Med. Biol.* **2023**, *5*, 421–427. [\[CrossRef\]](#)
48. Cortinhal, T.; Tzelepis, G.; Erdal Aksoy, E. Salsanext: Fast, uncertainty-aware semantic segmentation of lidar point clouds. In Proceedings of the Advances in Visual Computing: 15th International Symposium, ISVC 2020, San Diego, CA, USA, 5–7 October 2020; Proceedings, Part II 15; pp. 207–222.
49. Zhang, Y.; Zhang, Q.; Zhu, Z.; Hou, J.; Yuan, Y. Glenet: Boosting 3d object detectors with generative label uncertainty estimation. *Int. J. Comput. Vis.* **2023**, *131*, 3332–3352. [\[CrossRef\]](#)
50. Consagra, W.; Ning, L.; Rathi, Y. Neural orientation distribution fields for estimation and uncertainty quantification in diffusion MRI. *Med. Image Anal.* **2024**, *93*, 103105. [\[CrossRef\]](#)
51. Lin, F.; Yue, Y.; Zhang, Z.; Hou, S.; Yamada, K.; Kolachalama, V.; Saligrama, V. InfoCD: A Contrastive Chamfer Distance Loss for Point Cloud Completion. In *Advances in Neural Information Processing Systems*; Oh, A., Naumann, T., Globerson, A., Saenko, K., Hardt, M., Levine, S., Eds.; Curran Associates, Inc.: San Francisco, CA, USA, 2023; Volume 36, pp. 76960–76973.
52. Bartoň, M.; Hanniel, I.; Elber, G.; Kim, M.S. Precise Hausdorff distance computation between polygonal meshes. *Comput. Aided Geom. Des.* **2010**, *27*, 580–591. [\[CrossRef\]](#)
53. Rote, G. Computing the minimum Hausdorff distance between two point sets on a line under translation. *Inf. Process. Lett.* **1991**, *38*, 123–127. [\[CrossRef\]](#)

54. Powers, D.M. Evaluation: From precision, recall and F-measure to ROC, informedness, markedness and correlation. *arXiv* **2020**, arXiv:2010.16061.
55. Im, J.; Kim, J.Y.; Yu, H.S.; Lee, K.J.; Choi, S.H.; Kim, J.H.; Ahn, H.K.; Cha, J.Y. Accuracy and efficiency of automatic tooth segmentation in digital dental models using deep learning. *Sci. Rep.* **2022**, *12*, 9429. [[CrossRef](#)]
56. Wu, T.H.; Lian, C.; Lee, S.; Pastewait, M.; Piers, C.; Liu, J.; Wang, F.; Wang, L.; Chiu, C.Y.; Wang, W.; et al. Two-stage mesh deep learning for automated tooth segmentation and landmark localization on 3D intraoral scans. *IEEE Trans. Med. Imaging* **2022**, *41*, 3158–3166. [[CrossRef](#)]
57. Ning, X.; Li, F.; Tian, G.; Wang, Y. An efficient outlier removal method for scattered point cloud data. *PLoS ONE* **2018**, *13*, e0201280. [[CrossRef](#)]
58. Gomes, J.; Kong, J.; Kurc, T.; Melo, A.C.; Ferreira, R.; Saltz, J.H.; Teodoro, G. Building robust pathology image analyses with uncertainty quantification. *Comput. Methods Programs Biomed.* **2021**, *208*, 106291. [[CrossRef](#)]
59. Yuan, Y.; Wu, Y.; Fan, X.; Gong, M.; Miao, Q.; Ma, W. Inlier Confidence Calibration for Point Cloud Registration. In Proceedings of the IEEE/CVF Conference on Computer Vision and Pattern Recognition (CVPR), Seattle, DC, USA, 19–21 June 2024; pp. 5312–5321.
60. Zhang, L.; Yang, A.J.; Xiong, Y.; Casas, S.; Yang, B.; Ren, M.; Urtasun, R. Towards unsupervised object detection from lidar point clouds. In Proceedings of the IEEE/CVF Conference on Computer Vision and Pattern Recognition, Vancouver, BC, Canada, 18–22 June 2023; pp. 9317–9328.
61. Ghesu, F.C.; Georgescu, B.; Zheng, Y.; Grbic, S.; Maier, A.; Hornegger, J.; Comaniciu, D. Multi-scale deep reinforcement learning for real-time 3D-landmark detection in CT scans. *IEEE Trans. Pattern Anal. Mach. Intell.* **2017**, *41*, 176–189. [[CrossRef](#)]
62. Su, J.; Li, S.; Wolff, L.; van Zwam, W.; Niessen, W.J.; van der Lugt, A.; van Walsum, T. Deep reinforcement learning for cerebral anterior vessel tree extraction from 3D CTA images. *Med. Image Anal.* **2023**, *84*, 102724. [[CrossRef](#)]
63. Choi, S.; Jang, S.; Jung, S.; Cho, H.J.; Jeon, B. Deep Reinforcement Learning for Efficient Registration between Intraoral-Scan Meshes and Ct Images. *Available at SSRN 4818934* **2023**. Available online: https://papers.ssrn.com/sol3/papers.cfm?abstract_id=4818934 (accessed on 18 September 2024).

Disclaimer/Publisher’s Note: The statements, opinions and data contained in all publications are solely those of the individual author(s) and contributor(s) and not of MDPI and/or the editor(s). MDPI and/or the editor(s) disclaim responsibility for any injury to people or property resulting from any ideas, methods, instructions or products referred to in the content.